RSC Advances

PAPER

View Article Online
View Journal | View Issue

Cite this: *RSC Adv.*, 2020, **10**, 42340

A fungus-derived biomass porous carbon–MnO_2 nanocomposite-modified electrode for the voltammetric determination of rutin

Hui Cheng,[ab] Juan Liu,[b] Yunxiu Sun,[b] Ting Zhou,[a] Qiuyue Yang,[a] Shuyao Zhang,[a] Xiaoping Zhang,[*a] Guangjiu Li*[b] and Wei Sun[a]

Received 1st July 2020
Accepted 3rd October 2020

DOI: 10.1039/d0ra05739h

rsc.li/rsc-advances

In this study, we designed a simple procedure for the synthesis of fungus-derived biomass porous carbon (FBPC), which was further used to prepare a MnO_2@FBPC composite by a hydrothermal method. The MnO_2@FBPC nanocomposite showed a porous structure, large specific surface area, and high conductivity, and was modified on the carbon ionic liquid electrode (CILE) to obtain a working electrode for the sensitive voltammetric determination of rutin. The electrochemical response of rutin was studied *via* cyclic voltammetry with electrochemical parameters calculated. Under the optimal conditions, the linear range for the rutin analysis was obtained by the differential pulse voltammetry from 0.008 to 700.0 μmol L^{-1} with the detection limit of 2.67 nmol L^{-1} (3σ). This MnO_2@FBPC/CILE was applied to directly detect the rutin concentration in drug and human urine samples with satisfactory results.

1 Introduction

Rutin is one of the most important flavonoid glycoside compounds that is widely present in legumes, vegetables, fruits, nuts, and seeds of plants.[1] Due to the physiological activities such as anti-inflammatory, anti-bacterial, and anti-tumor,[2–4] rutin has been used in pharmaceutical applications. Therefore, it is necessary to develop sensitive methods to detect the rutin content in various samples. Numerous analytical techniques have been established for the analysis of rutin, such as capillary electrophoresis,[5] adsorptive stripping voltammetry,[6] chemiluminescence,[7] high-performance liquid chromatography,[8] sequential injection analysis,[9] and spectrophotometry.[10] However, some of these techniques exhibit shortcomings including time-consuming, high cost, and complicated operation processes. Among these methods, electrochemical procedures have been applied to rutin detection due to its high sensitivity, convenient and fast procedure, cheap instrumentation, and on-site monitoring.[11] For example, He *et al.* fabricated an electrochemical sensor for the rutin detection based on amine-functionalized Fe_3O_4 nanoparticles and electrochemically reduced graphene oxide nanocomposite-modified glassy carbon electrode.[12] Apetrei *et al.* presented a graphene–gold nanoparticle-based screen-printed voltammetric sensor for the determination and quantification of rutin in pharmaceutical samples.[13] Xing *et al.* presented a gold nanoparticle-loaded ZnS nanocomposite-based voltammetric sensor for the sensitive determination of rutin.[14] Niu *et al.* constructed a graphene and gold nanoparticle-modified acupuncture needle electrode to detect the concentration of rutin.[15] Sun *et al.* synthesized a graphene–MnO_2 nanocomposite-modified electrode for the sensitive determination of rutin.[16] Among the modified electrodes reported for rutin detection, numerous types of nanocomposites have been synthesised and used as modifiers that can adsorb more rutin on the electrode surface, exhibit fast electron transfer rate for rutin electrochemistry, and show certain electrocatalytic activity towards rutin. However, the modifiers have disadvantages such as expensive raw materials or complicated synthesis procedures.

Biomass porous carbon (BPC) is defined as a carbon-rich, porous solid produced by the thermal decomposition of biomass in a reactor with little or no available air at moderate temperatures.[17] It has received considerable attention in the fields of environment, energy, and sensing due to its large active surface areas, pore volumes, cheap price, high chemical, and thermal stability.[18,19] Recently, numerous synthetic methods have been proposed to prepare porous carbon by the pyrolysis of biomass in the presence of chemical agents such as KOH, $ZnCl_2$, and H_3PO_4.[20] For example, Sevilla *et al.* prepared nitrogen-doped porous carbon with a surface area of up to 3480 m^2 g^{-1} by the KOH activation of polypyrrole as a carbon source.[21] Chang *et al.* synthesised biomass-activated carbon *via* the $ZnCl_2$ chemical activation of a recycled filter paper with specific capacitance as high as 302.3 F g^{-1}.[22] Dai *et al.* prepared argy wormwood-based

[a]*Key Laboratory of Laser Technology and Optoelectronic Functional Materials of Hainan Province, College of Chemistry and Chemical Engineering, Hainan Normal University, Haikou 571158, P. R. China. E-mail: 254787885@qq.com*

[b]*Key Laboratory of Optic-electric Sensing and Analytical Chemistry for Life Science of Ministry of Education, Shandong Key Laboratory of Biochemical Analysis, College of Chemistry and Molecular Engineering, Qingdao University of Science and Technology, Qingdao 266042, P. R. China. E-mail: lgjqust@126.com*

porous carbon electrode materials through H_3PO_4 pre-treatment, hydrothermal carbonization, and subsequent KOH activation for high-performance supercapacitors.[23]

The electrode material is a major factor that affects the performance of electrochemical sensors. Numerous types of metal oxides have been used as electrode materials.[24–27] As an attractive inorganic semiconductive material with electrocatalytic ability, MnO_2 has aroused widespread concern in sensing electrodes owing to its low toxicity, inexpensive cost, wide potential range, natural abundance, and high specific capacitance.[28,29] Also, MnO_2 can be combined with other conductive materials to get composites with improved conductivity.[30] Jafta *et al.* prepared an asymmetric electrochemical device with an MnO_2/graphene oxide composite by a hydrothermal reaction.[31] Yuan *et al.* prepared an excellent electrochemical supercapacitor with MnO_2 and rice husk-based carbon composite as the active material.[32]

In this study, fungus was used as the raw material to prepare fungus-derived biomass porous carbon (FBPC) by alkali-treatment activation and carbonization. Then, the hydrothermal method was used to get an MnO_2 decorated FBPC composite MnO_2@FBPC, which was further applied on the top of a carbon ionic liquid electrode (CILE) to obtain the modified electrode. CILE is prepared by using a highly conductive ionic liquid (IL) as the modifier, which has been used as the basic electrode in electroanalysis due to its specific characteristics such as faster electron transfer, higher stability, and wider potential window. Our group fabricated numerous types of modified electrodes using CILE for electrochemical sensors and electrocatalysis.[33–37] Therefore, CILE is used as the substrate electrode with the MnO_2@FBPC nanocomposite as the modifier. The electrochemical responses of rutin on MnO_2@FBPC/CILE were investigated *via* cyclic voltammetry (CV) and differential pulse voltammetry (DPV) with electrochemical parameters calculated. The modified electrode was further applied for the analysis of samples with satisfactory results.

2 Materials and methods

2.1 Reagents

1-Hexylpyridinium hexafluorophosphate ($HPPF_6$ > 99%, Lanzhou Yulu Fine Chemical Co., Ltd., China), graphite powder (average particle size 30 μm, Shanghai Colloid Chemical Co., China), $KMnO_4$ (Tianjin Zhiyuan Chemical Reagent Co., Ltd., China), $MnSO_4 \cdot H_2O$ (Guangdong Xiqiao Chemical Co., Ltd., China), rutin (Sinopharm Chemical Reagent Co., Ltd., China) and rutin tablet sample (Shanxi Yunpeng Pharmaceutical Co., Ltd., China, and Shanghai Zhaohui Pharmaceutical Co., Ltd., China) were used as received. Fungus was purchased from a local agricultural market of Haikou. A 0.1 mol L^{-1} phosphate buffer solution (PBS) with different pH values was used as a supporting electrolyte. All the other chemicals were of analytical reagent grade without further purification, and ultrapure water (Milli-Q, IQ-7000, USA) was used in all the experiments.

2.2 Instruments

The morphologies of the as-prepared materials were examined using a JSM-7100F scanning electron microscope (JEOL, Japan). X-ray diffraction (XRD) measurements were performed on a D2 phaser advance diffractometer (Bruker, Germany) with Cu Kα (λ = 1.5406 nm) radiation. X-ray photoelectron spectroscopy (XPS) and the surface elemental compositions were performed on an AXIS HIS 165 spectrometer (Kratos Analytical, UK). Raman spectrum was obtained on a LabRAM HR system (Horiba, France) at an excitation wavelength of 532 nm. Electrochemical measurements were carried out on a CHI 660E electrochemical workstation (Shanghai CH Instruments, China) with a traditional three-electrode system, including MnO_2@FBPC/CILE as the working electrode, Ag/AgCl (saturated KCl) as the reference electrode, and a platinum wire electrode as the counter electrode. An Agilent 1200 (Agilent Technologies, USA) was used for HPLC with chromatographic separation performed on the Agilent Diamonsil C18 column (250 mm × 4.6 mm, 5 μm, USA). HPLC mobile phase consisted of a 0.4% phosphoric acid–methanol (48 : 52, v/v) mixture, which was filtered through a 0.45 μm filter, followed by degassing under vacuum and passed at a flow rate of 0.5 mL min^{-1} at an injection volume of 10 μL. The measurement process was carried out in a chromatographic column at 30 °C with the detector wavelength set at 368 nm.

2.3 Synthesis of FBPC

The fungus was washed with water and dried at 100 °C for 12 h. Then, 2.0 g fungus was mixed with 50 mL of 0.1 mol L^{-1} KOH, transferred into a Teflon lined stainless-steel autoclave (100 mL), and heated at 120 °C for 6 h. After the product was cooled to room temperature naturally and dried at 100 °C for 24 h, the sample was heated in a KMTF-100 tube furnace (Anhui Kemi Instruments, China) under an Ar flow at 800 °C (10 °C min^{-1}) for 1 h. Finally, the sample was washed three times with water and 1.0 mol L^{-1} HCl, respectively, until the pH of the solution reached 7.0. Then, the product was dried at 100 °C in an oven for 12 h to obtain FBPC.

2.4 Synthesis of MnO_2@FBPC

The MnO_2@FBPC composite was synthesized by a hydrothermal method.[38] Briefly, 0.17 g $KMnO_4$, 0.28 g $MnSO_4$, and 0.24 g FBPC were dispersed in 10 mL water to form a homogeneous solution under constant magnetic stirring. Then, the mixture was transferred into a Teflon lined stainless-steel autoclave and heated at 140 °C for 12 h. The sample was filtered and washed three times with water and dried at 60 °C for 12 h to obtain MnO_2@FBPC.

2.5 Preparation of the modified electrode

According to the previous literature,[39] CILE was prepared with $HPPF_6$ and graphite powder, which was smoothed to a mirror-like surface before use. 2.0 mg mL^{-1} of the MnO_2@FBPC suspension was sonicated for 4 h to obtain a uniform dispersion. Then, 8.0 μL of the MnO_2@FBPC suspension was cast on the CILE surface and dried at room temperature in air to construct MnO_2@FBPC/CILE.

3 Results and discussion

3.1 Principles

Scheme 1 illustrates the fabrication process of the MnO_2@FBPC composite, which was modified on the surface of CILE and used for the rutin analysis. The fungus is activated in 0.1 mol L^{-1} KOH and then carbonized at 800 °C to form a loose and porous structure. Subsequently, MnO_2 nanoneedles are formed on FBPC by the hydrothermal method. The as-prepared materials are used for electrode modification, and the electrochemical behaviour of rutin is further investigated on the MnO_2@FBPC modified electrode.

3.2 Characterization of MnO_2@FBPC

SEM images of FBPC and MnO_2@FBPC were recorded and are exhibited in Fig. 1. As for FBPC (Fig. 1A), a tubular channel and three-dimensional porous structure could be observed, which was attributed to activation by KOH and further high-temperature carbonization. This porous structure can provide a good interface for the further attachment or growth of other nanomaterials on and inside its structure. As for MnO_2@FBPC, MnO_2 nanoneedles could be observed on the FBPC surface (Fig. 1B and C). The possible formation mechanism of MnO_2 can be described with the following chemical equation:

$$3MnSO_4 + 2KMnO_4 + 2H_2O \rightarrow 5MnO_2 + 2H_2SO_4 + K_2SO_4.$$

Raman spectroscopy is an effective approach to study the structure of carbon materials and the curves are shown in Fig. 1D. The characteristic peaks of the Raman spectrum are located at 1603 cm^{-1} and 1337 cm^{-1} (curve a and b), which are attributed to the G and D bands of the carbon material, respectively. Because the intensity ratio of I_D/I_G represents the disorder/defect degree of the carbon material, the I_D/I_G values of FBPC and MnO_2@FBPC were obtained as 1.2 and 0.7, respectively. Obviously, the I_D/I_G value decreased in the presence of MnO_2 nanoneedles, indicating a relatively high degree of graphitization. Compared with that of FBPC, a new peak could be found at 631 cm^{-1} (curve b), which belonged to the characteristic peak of MnO_2.

XRD patterns were recorded to determine the crystal structure of FBPC and MnO_2@FBPC, and the curves are shown in Fig. 1E. In the XRD pattern of FBPC (curve a), two typical diffraction peaks at 2θ values of 29.1° and 42.4° could be ascribed to reflections from the (002) and (110) crystal planes of the carbon material. For the MnO_2@FBPC nanocomposite, strong diffraction peaks appeared at 18.0°, 22.4°, 28.7°, 37.6°, 41.9°, 49.8°, 56.0°, 60.1°, and 65.5°, which were attributed to the (200), (220), (310), (211), (301), (411), (600), (521), and (002) crystal faces of MnO_2. Therefore, the MnO_2 crystal face is retained in MnO_2@FBPC.

XPS was performed to obtain the elemental composition of FBPC and MnO_2@FBPC, and the resulting curves are shown in Fig. 1F. The C 1s spectra were fitted with five component peaks, as shown in Fig. 1G. The peaks located at 284.78 eV, 286.38 eV, 288.38 eV, 292.02 eV and 294.78 eV are attributed to the structure of graphite carbon (C–C), carbon–oxygen (C–O), carboxyl group (C═O), K $2p_{2/3}$ and K $2p_{1/2}$, respectively. The characteristic peaks (529.80 eV, 531.28 eV, and 532.72 eV) of O 1s indicated that the structures of Mn–O, C–O, and C═O, respectively, as shown in Fig. 1H existed in the composite. Mn 2p was combined with the fitted peaks (642.00 eV and 643.90 eV) of Mn $2p_{2/3}$ and the fitted peaks (653.40 eV and 654.70 eV) of Mn $2p_{1/2}$. Therefore, it was concluded that MnO_2 was synthesized and coated on FBPC. Moreover, the atomic ratio of Mn in the MnO_2@FBPC composite was calculated as 9.95%.

3.3 Electrochemical investigations

Cyclic voltammetric responses of different electrodes were recorded using a 1.0 mmol L^{-1} $[Fe(CN)_6]^{3-}$ solution as an

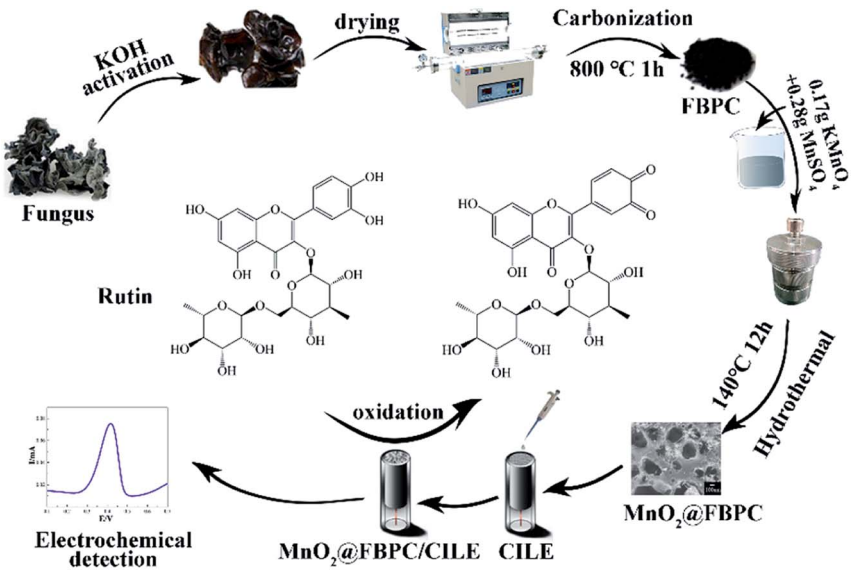

Scheme 1 Fabrication process of MnO_2@FBPC composites and the electrochemical detection of rutin.

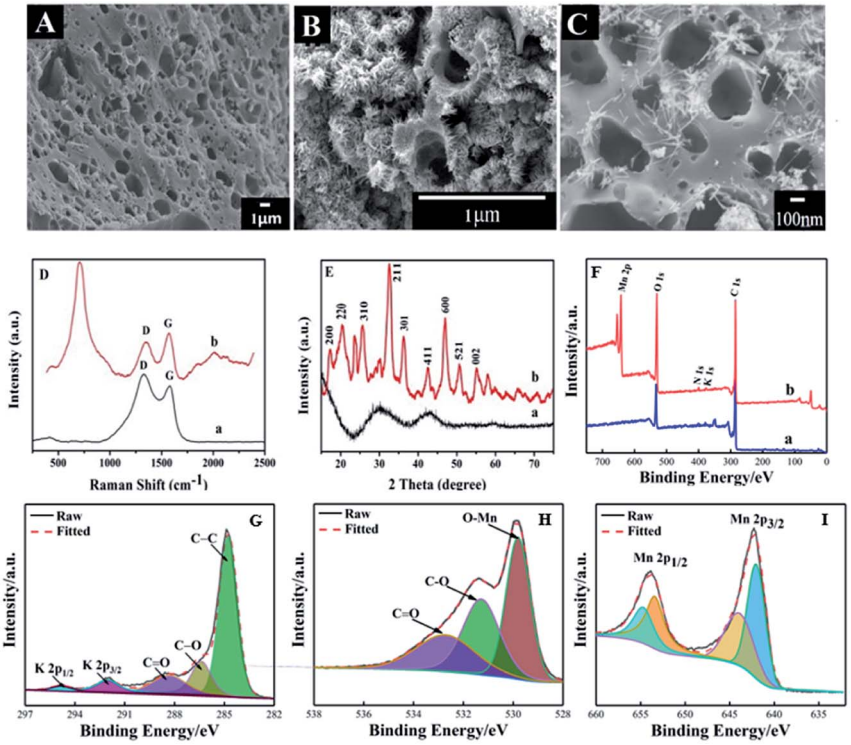

Fig. 1 SEM images of (A) FBPC and (B and C) MnO_2@FBPC at various magnification, (D) Raman spectra, (E) XRD survey and (F) XPS patterns of FBPC (a) and MnO_2@FBPC (b); XPS spectra of the MnO_2@FBPC (G) C 1s, (H) O 1s, (I) Mn 2p.

electrochemical probe, and the results are shown in Fig. 2A. A pair of symmetric redox peaks could be observed on bare CILE (curve a), and the redox peaks increased gradually on FBPC/CILE (curve b) and MnO_2@FBPC/CILE (curve c), indicating that the highly conductive FBPC and MnO_2@FBPC composite were beneficial for the electron transfer and further effectively improved the interfacial conductivity. The linear relationships between I_p and the square-root of the scan rate ($v^{1/2}$) was obtained with the equations as I_{pc} (μA) $= 46.408v^{1/2} - 14.348$ ($n = 17$, $\gamma = 0.992$) and I_{pa} (μA) $= -40.043v^{1/2} + 11.628$ ($n = 17$, $\gamma = 0.990$). According to the Randles–Sevcik formula, I_{pa} (A) $= (2.69 \times 10^5)n^{3/2}AD^{1/2}C_0v^{1/2}$,[40] the effective surface area (A) of MnO_2@FBPC/CILE was calculated to be 0.241 cm^2, which was 1.67 times larger than that of CILE (0.144 cm^2), indicating that the presence of the MnO_2@FBPC composite on the electrode increased the effective area and provided more active sites on the electrochemical surface with improved electrode performance.

To get the impedance information, electrochemical impedance spectroscopy (EIS) was performed in a 10 mmol L^{-1} $[Fe(CN)_6]^{3-}$ and 0.5 mol L^{-1} KCl solution with frequency ranging from 10^4 to 0.1 Hz. The experimental data were fitted by the R(CR)(CR) model in Fig. 2B. The R_{et} of MnO_2@FBPC/CILE (35.0 Ω, curve a) was smallest among those of three electrodes, and the R_{et} of FBPC/CILE (182.3 Ω, curve b) was lower than that of CILE (302.4 Ω, curve c), indicating an improved electron transfer, which was attributed to the presence of porous FBPC and MnO_2.

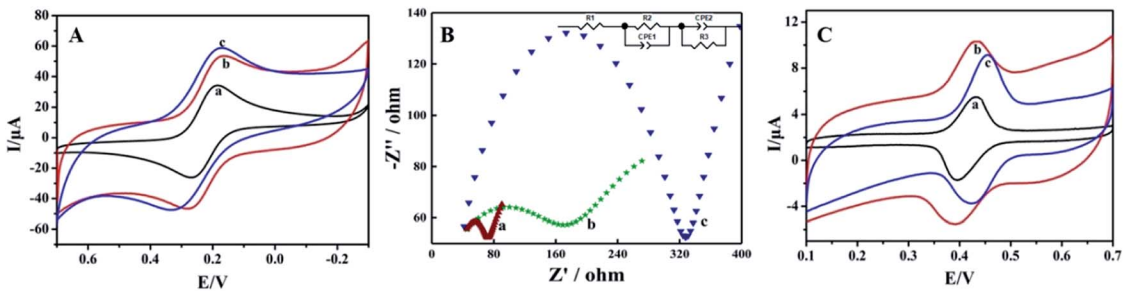

Fig. 2 (A) Cyclic voltammograms of CILE (a), FBPC/CILE (b) and MnO_2@FBPC/CILE (c) in 1.0 mmol L^{-1} $[Fe(CN)_6]^{3-}$ and 0.5 mol L^{-1} KCl solution at a scan rate of 100 mV s^{-1}. (B) EIS of MnO_2@FBPC/CILE (a), FBPC/CILE (b) and CILE (c) in 10.0 mmol L^{-1} $[Fe(CN)_6]^{3-}$ and 0.5 mol L^{-1} KCl solution with frequency ranging from 10^4 to 0.1 Hz. (C) Cyclic voltammograms of 1.0×10^{-5} mol L^{-1} rutin in PBS (pH 4.0) on CILE (a), FBPC/CILE (b) and MnO_2@FBPC/CILE (c) at a scan rate of 100 mV s^{-1}.

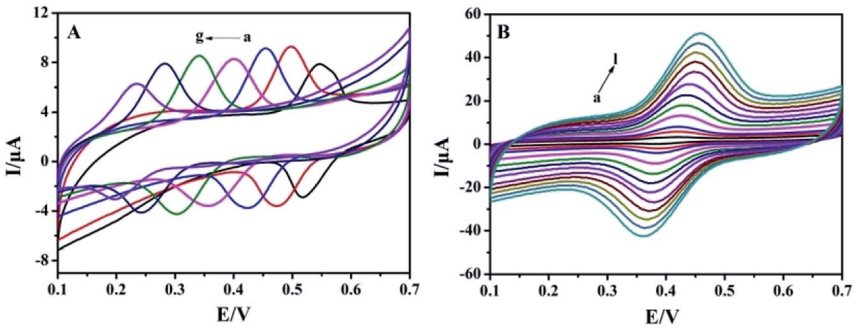

Fig. 3 Cyclic voltammograms of 1.0×10^{-5} mol L^{-1} rutin on MnO_2@FBPC/CILE with (A) different pH PBS (a–g: 2.0, 3.0, 4.0, 5.0, 6.0, 7.0, 8.0) at the scan rate of 100 mV s; (B) different scan rates in pH 4.0 PBS (a–l: as 20, 60, 100, 200, 300, 400, 500, 600, 700, 800, 900, 1000 mV s^{-1}).

The electrochemical behaviour of 1.0×10^{-5} mol L^{-1} rutin on different electrodes was studied *via* CV in PBS (0.1 mol L^{-1}, pH 4.0), and the curves are shown in Fig. 2C. A couple of well-defined redox peaks could be observed, which was the typical electrochemical reaction of rutin. On CILE, the peak currents were obtained as 3.206 μA (I_{pa}) and 3.268 μA (I_{pc}) with the peak-to-peak separation (ΔE_p) of 35 mV (curve a). On FBPC/CILE, the redox peak currents of rutin were increased to 4.100 μA (I_{pa}) and 3.474 μA (I_{pc}) with ΔE_p as 39 mV (curve b), proving the positive effect of FBPC to the rutin electrochemistry. Also, the increase in the background currents was due to the porous structure and large surface area of FBPC, indicating that the presence of the porous structure increased the interfacial capacitance. Moreover, on MnO_2@FBPC/CILE (curve c), the electrochemical responses were further increased with the decrease of ΔE_p to 31 mV, indicating that the redox reaction of rutin become more reversible. The corresponding redox peak currents were 5.338 μA (I_{pa}) and 3.997 μA (I_{pc}), and the currents were enlarged 1.7 times for I_{pa} and 1.2 times for I_{pc}, as compared to that of CILE. The modification of MnO_2 nanoneedles on the surface of FBPC significantly increased the electrocatalytic activity towards the oxidation of rutin with the enhancement of the electrochemical responses. Therefore, the presence of the high conductivity of MnO_2@FBPC promoted the electron transfer ability towards rutin.

3.4 Effect of pH and scan rate

The effect of buffer pH on the electrochemical responses of 1.0×10^{-5} mol L^{-1} rutin on MnO_2@FBPC/CILE was investigated, and the results are shown in Fig. 3A. With the change in pH from 2.0 to 8.0, the redox peak potential shifted towards the negative direction and the peak current achieved a maximum value at pH 4.0, which was selected as the supporting electrolyte. The formal peak potential ($E^{0\prime}$) had a good linear relationship with the pH value and the regression equation was $E^{0\prime}$ (V) = −0.054 pH + 0.65 ($n = 7$, $\gamma = 0.998$). The slope of 54 mV pH^{-1} was close to 59 mV pH^{-1}, which suggested that the number of electrons transferred was equal to the protons in the electrode reaction process.

The effect of the scan rate on the redox response of 1.0×10^{-5} mol L^{-1} rutin was recorded, and the results are shown in Fig. 3B. The redox peak currents increased gradually with the increase in the scan rate in the range from 20 mV s^{-1} to 1000 mV s^{-1}, and the linear relationship of peak currents and scan rate were I_{pa} (μA) = 32.64υ (V s^{-1}) + 1.13 ($n = 13$, $\gamma = 0.997$) and I_{pc} (μA) = −28.81υ (V s^{-1}) − 1.11 ($n = 13$, $\gamma = 0.998$), which indicated that the electrode reaction was an adsorption-controlled process due to the porous structure of FBPC. The redox peak potential and ln υ also exhibited good linear relationships with the linear regression equations, as E_{pa} (V) = 0.023 ln υ + 0.458 ($n = 8$, $\gamma = 0.990$) and E_{pc} (V) = −0.025 ln υ + 0.358 ($n = 8$, $\gamma = 0.994$). According to the Laviron's equation,[41] the values of the electron transfer coefficient (α), electron transfer number (n), and electrode reaction standard rate constant (k_s) were calculated as 0.48, 2.14, and 4.65 s^{-1}, respectively.

3.5 Effects of accumulation conditions

To improve the detection sensitivity, the effects of accumulation time and potential on the oxidation peak current were

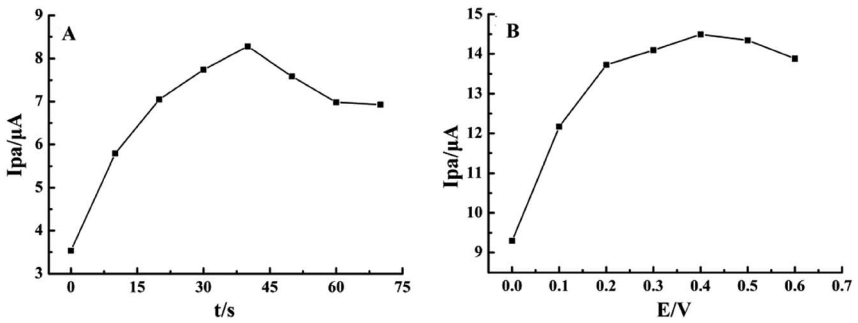

Fig. 4 Effects of (A) accumulation time and (B) potential on I_{pa} of 1.0×10^{-5} mol L^{-1} rutin on MnO_2@FBPC/CILE.

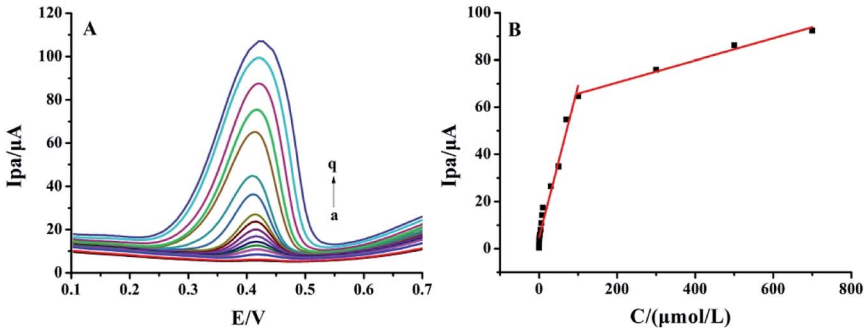

Fig. 5 DPV curves of rutin with various concentrations (A) a–q: 0.008, 0.01, 0.1, 0.6, 1.0, 2.0, 4.0, 6.0, 8.0, 10.0, 30.0, 50.0, 70.0, 100.0, 300.0, 500.0, 700.0 μmol L^{-1}. (B) The linear relationship between I_{pa} and rutin concentration.

Table 1 Comparison of various modified electrodes for rutin detection

Electrodes	Linear range (μmol L^{-1})	LOD (μmol L^{-1})	Ref.
PABSA[a]/GCE[b]	0.25–10.0	0.0012	42
GR[c]–MnO_2/CILE	0.01–500.0	0.0027	43
Ni–GO[d]/GCE	0.011–15.0	0.0032	44
Cu_2O–Au[e]/NG[f]/GCE	0.06–512.9	0.03	45
Au–AgNT[g]/NG	0.79–61.0	0.16	46
PdPc–MWCNT[h]–Nafion/GCE	0.1–51.0	75.0	47
MWNTs[i]/β-CD[j]/GCE	0.4–1000.0	0.2	48
MnO_2@FBPC/CILE	0.008–700.0	0.00267	This work

[a] Poly(*p*-aminobenzene sulfonic acid). [b] Glassy carbon electrode. [c] Graphene. [d] Nickel nanoparticle–graphene oxide. [e] Cuprous-oxide–Au nanoparticles. [f] N-doped graphene. [g] Au–Ag nanoparticles. [h] Palladium phthalocyanine–multiwalled carbon nanotube. [i] Multiwall carbon nanotubes. [j] β-Cyclodextrin.

investigated, as shown in Fig. 4. I_{pa} increased rapidly with the accumulation time from 0 s to 40 s and then decreased by more than 40 s, indicating the saturated adsorption of rutin (Fig. 4A). Simultaneously, I_{pa} increased with the increase in the accumulation potential from 0 V to 0.4 V and gradually decreased when the accumulation potential was more than 0.4 V (Fig. 4B). Therefore, 40 s and 0.4 V were chosen as the optimal accumulation conditions in the subsequent experiments.

3.6 Calibration curve

Differential pulse voltammetric (DPV) curves of different rutin concentrations on MnO_2@FBPC/CILE are shown in Fig. 5A. The oxidation peak currents increased with rutin in two concentration ranges, *i.e.*, from 0.008 to 100.0 μmol L^{-1} and 100.0 to 700.0 μmol L^{-1}. The linear regression equations were calculated as I_{pa} (μA) = 0.643C (μmol L^{-1}) + 4.733 (n = 14, γ = 0.996) and I_{pa} (μA) = 0.047C (μmol L^{-1}) + 61.095 (n = 4, γ = 0.992) with the detection limit calculated as 2.67 nmol L^{-1} (3σ). Two different slopes of the calibration curves could be attributed to the difference in the activity of the modified electrode surface at low and high rutin concentrations. At the low concentration range, a large slope was due to the relatively high ratio of active sites to the total number of rutin molecules. At the high concentration range, the active sites decreased in comparison to the total number of rutin molecules at the electrode surface, leading to a smaller slope value. The analytical parameters for the electrochemical detection of rutin on different modified electrodes are summarized in Table 1. The low detection limit was due to the presence of MnO_2 on the surface of FBPC with a porous structure, larger surface area, high conductivity, and excellent electrocatalytic activity.

3.7 Analytical applications

In order to verify the practicality and reliability of the proposed sensor, MnO_2@FBPC/CILE was applied for the determination of rutin content in compound rutin tablets (20 mg per tablet) and human urine by the calibration curve method and standard addition method. Drug tablets were purchased from Shanxi Yunpeng Pharmaceutical Ltd. Co. (B080302) and Shanghai Zhaohui Pharmaceutical Ltd. Co. (090904). A piece of drug tablet was ground and dissolved in 5.0 mL ethanol to obtain a 6.02 mmol L^{-1} stock solution. Then, a 100 μL stock solution was diluted with pH 4.0 PBS in a 10.0 mL calibration tube for

Table 2 Detection of rutin in different samples with MnO_2@FBPC/CILE (n = 3)

Sample	Labeled (μmol L^{-1})	Found (μmol L^{-1})	Added (μmol L^{-1})	Measured (μmol L^{-1})	RSD (%)	Recovery (%)
B080302	60.20	59.18	20.00	80.67	2.18	107.46
090904	60.20	60.03	60.00	121.96	3.23	103.22
Normal human urine	—	0.00	20.00	18.49	4.79	92.45
			40.00	42.01	5.95	105.03
			60.00	59.05	1.69	98.42

Table 3 Influence of co-existing substances on 1.0×10^{-5} mol L^{-1} rutin analysis

Co-exiting species	Concentration (mol L^{-1})	RE (%)	Co-exiting species	Concentration (mol L^{-1})	RE (%)
KCl	5.0×10^{-4}	5.18	$BaCl_2$	5.0×10^{-4}	2.82
NaCl	5.0×10^{-4}	2.87	$CoCl_2$	5.0×10^{-4}	7.16
$CaCl_2$	5.0×10^{-4}	2.16	Bisphenol A	1.0×10^{-5}	6.65
Glucose	5.0×10^{-4}	2.87	Ascorbic acid	1.0×10^{-5}	1.63
Alanine	5.0×10^{-4}	−0.62	Catechol	1.0×10^{-5}	2.86
Glutamine	5.0×10^{-4}	2.99	Hydroquinone	1.0×10^{-5}	8.03
Uric acid	5.0×10^{-4}	3.36	Baicalin	1.0×10^{-5}	6.73
Dopamine	5.0×10^{-4}	−3.74	Luteolin	1.0×10^{-5}	3.07

further detection. Drug samples were also detected by the HPLC method based on the ref. 49 with the average value as 62.29 μmol L^{-1}, which was close to the electrochemical data (shown in Table 2). The human urine sample (from health volunteer) was collected and the supernatant from the static solution was removed. Then, 0.1 mL sample was further diluted to 10.0 mL with pH 4.0 PBS, detected by the proposed procedure with the addition of a standard rutin solution to test the recovery, which was in the range of 92.45–105.03%. All the above results confirmed that MnO_2@FBPC/CILE could be efficiently applied for rutin detection with good accuracy.

3.8 Interferences study

The influence in a number of inorganic ions, amino acids, glucose, and some flavonoid drugs on the detection of 1.0×10^{-5} mol L^{-1} rutin was also investigated. As shown in Table 3, it can be seen that higher concentrations (by 50 times) of inorganic ions, amino acids, glucose, uric acid, and dopamine led to the relative error (RE) less than 7.50%. Similar concentrations of bisphenol A, ascorbic acid, catechol, hydroquinone, baicalin, and luteolin had a relative error of less than 8.0%. Therefore, this MnO_2@FBPC/CILE may be used for the analysis of the rutin content in drug or biological samples.

3.9 Reproducibility, repeatability, and stability

The reproducibility of MnO_2@FBPC/CILE was performed by detecting the 1.0×10^{-5} mol L^{-1} rutin solution. The RSD value of six parallel measurements with a single electrode was calculated as 6.98%, indicating the good reproducibility of this method. In a series of five electrodes prepared in the same way, an RSD of 2.40% was obtained for the 1.0×10^{-5} mol L^{-1} rutin solution, indicating excellent repeatability. The long-term stability of MnO_2@FBPC/CILE was tested after being stored at room temperature for a week. The current responses were retained at 90% of its original signal strengths for the same rutin solution, which showed long-term stability.

4 Conclusions

The fungus-based biomass porous carbon (FBPC) was prepared by activation and high temperature carbonization, and the MnO_2@FBPC composite was directly synthesised by a hydrothermal method. The morphology, structure, and composition of the materials were characterized by SEM, Raman, XRD, and XPS. The results showed that the MnO_2@FBPC composite had a porous structure, large surface area, good conductivity, and high electrocatalytic activity. The electrochemical response of rutin on MnO_2@FBPC/CILE was investigated with the electrochemical parameters calculated, which exhibited a wider linear range (0.008–700.0 μmol L^{-1}) and lower detection limit for the rutin detection, and the method was successfully applied to the real sample detection. This work extended the usage of biomass porous carbon and the related composite in the field of electroanalysis.

Conflicts of interest

There are no conflicts to declare.

Acknowledgements

This work was financially supported by the Hainan Provincial Natural Science Foundation of China (2018CXTD336), the National Natural Science Foundation of China (61864002), the Open Foundation of Key Laboratory of Laser Technology and Optoelectronic Functional Materials of Hainan Province (2020LTOM01), and Open Project of Chemistry Department of Qingdao University of Science and Technology (QUSTHX201935).

References

1 J. B. He, Y. Wang, N. Deng, Z. G. Zha and X. Q. Lin, Cyclic voltammograms obtained from the optical signals: study of the successive electro-oxidations of rutin, *Electrochim. Acta*, 2007, **52**, 6665–6672.
2 R. M. Gené, C. Cartaña, T. Adzet, E. Marín, T. Parella and S. Cañigueral, Anti-inflammatory and analgesic activity of baccharis trimera: identification of its active constituents, *Planta Med.*, 1996, **62**, 232–235.
3 R. Ramanathan, N. Das and C. Tan, Inhibitory effects of 2-hydroxy chalcone and other flavonoids on human cancer cell-proliferation, *Int. J. Oncol.*, 1993, **3**, 115.
4 S. Yang, Q. U. Ling, L. I. Gang, Y. Ran and C. Liu, Gold nanoparticles/ethylenediamine/carbon nanotube modified glassy carbon electrode as the voltammetric sensor for

selective determination of rutin in the presence of ascorbic acid, *J. Electroanal. Chem.*, 2010, **645**, 115–122.

5 G. Chen, J. Zhang and J. H. Ye, Determination of puerarin, daidzein and rutin in Pueraria lobata (Wild.) Ohwi by capillary electrophoresis with electrochemical detection, *J. Chromatogr. A*, 2001, **923**, 255–262.

6 G. J. Volikakis and C. E. Efstathiou, Determination of rutin and other flavonoids by flow-injection/adsorptive stripping voltammetry using nujol-graphite and diphenylether-graphite paste electrodes, *Talanta*, 2000, **51**, 775–785.

7 S. Hartwell, Sensitive determination of sub-nanogram amounts of rutin by its inhibition on chemiluminescence with immobilized reagents, *Talanta*, 2002, **57**, 59–67.

8 K. Ishii, T. Furuta and Y. Kasuya, High-performance liquid chromatographic determination of quercetin in human plasma and urine utilizing solid-phase extraction and ultraviolet detection, *J. Chromatogr. B: Anal. Technol. Biomed. Life Sci.*, 2003, **794**, 49–56.

9 Z. Legnerová, Using on-line solid phase extraction for simultaneous determination of ascorbic acid and rutin trihydrate by sequential injection analysis, *Anal. Chim. Acta*, 2003, **497**, 165–174.

10 H. N. Hassan, B. N. Barsoum and I. H. Habib, Simultaneous spectrophotometric determination of rutin, quercetin and ascorbic acid in drugs using a kalman filter approach, *J. Pharm. Biomed. Anal.*, 1999, **20**, 315–320.

11 S. Hu, H. Zhu, S. Liu, J. Xiang, W. Sun and L. Zhang, Electrochemical detection of rutin with a carbon ionic liquid electrode modified by Nafion, graphene oxide and ionic liquid composite, *Microchim. Acta*, 2012, **178**, 211–219.

12 Q. He, J. Liu, X. Liu, G. Li, D. Chen, P. Deng and L. Jing, Fabrication of amine-modified magnetite-electrochemically reduced graphene oxide nanocomposite modified glassy carbon electrode for sensitive dopamine determination, *Nanomaterials*, 2018, **8**, 194.

13 I. M. Apetrei and C. Apetrei, A modified nanostructured graphene-gold nanoparticle carbon screen-printed electrode for the sensitive voltammetric detection of rutin, *Measurement*, 2018, **114**, 37–43.

14 R. Xing, X. Zhao, Y. Liu, J. Liu, B. Liu, Y. Ren, S. Liu and L. Mao, Low cost and reliable electrochemical sensor for rutin detection based on Au nanoparticles-loaded ZnS nanocomposites, *J. Nanosci. Nanotechnol.*, 2018, **18**, 4651–4657.

15 X. Niu, Z. Wen, X. Li, W. Zhao, X. Li and Y. Huang, Fabrication of graphene and gold nanoparticle modified acupuncture needle electrode and its application in rutin analysis, *Sens. Actuators, B*, 2018, **255**, 471–477.

16 S. Wei, X. Wang, H. Zhu, X. Sun, S. Fan, G. Li and Z. Sun, Graphene-MnO_2 nanocomposite modified carbon ionic liquid electrode for the sensitive electrochemical detection of rutin, *Sens. Actuators, B*, 2013, **178**, 443–449.

17 W. J. Liu, H. Jiang and H. Q. Yu, Development of biochar-based functional materials: toward a sustainable platform carbon material, *Chem. Rev.*, 2015, **115**, 12251–12285.

18 S. Mubeen, T. Zhang, B. Yoo, M. A. Deshusses and N. V. Myung, Palladium nanoparticles decorated single-walled carbon nanotube hydrogen sensor, *J. Phys. Chem. C*, 2007, **111**, 6321–6327.

19 J. Wang and L. Qian, Fungi-derived hierarchically porous carbons for high-performance supercapacitors, *RSC Adv.*, 2014, **5**, 4396–4403.

20 W. M. Qiao, S. H. Yoon and I. Mochida, KOH activation of needle coke to develop activated carbons for high-performance EDLC, *Energy Fuels*, 2006, **20**, 1680–1684.

21 M. Sevilla, R. Mokaya and A. B. Fuertes, Ultrahigh surface area polypyrrole-based carbons with superior performance for hydrogen storage, *Energy Environ. Sci.*, 2011, **4**, 2930.

22 B. Chang, Y. Guo, Y. Li and B. Yang, Hierarchical porous carbon derived from recycled waste filter paper as high-performance supercapacitor electrodes, *RSC Adv.*, 2015, **5**, 72019–72027.

23 C. Dai, J. Wan, J. Yang, S. Qu, T. Jin, F. Ma and J. Shao, H_3PO_4 solution hydrothermal carbonization combined with KOH activation to prepare argy wormwood-based porous carbon for high-performance supercapacitors, *Appl. Surf. Sci.*, 2018, **444**, 105–117.

24 W. Sun, Y. Guo, X. Ju, Y. Zhang, X. Wang and Z. Sun, Direct electrochemistry of hemoglobin on graphene and titanium dioxide nanorods composite modified electrode and its electrocatalysis, *Biosens. Bioelectron.*, 2013, **42**, 207–213.

25 W. Sun, X. Wang, Y. Wang, X. Ju, L. Xu, G. Li and Z. Sun, Application of graphene–SnO_2 nanocomposite modified electrode for the sensitive electrochemical detection of dopamine, *Electrochim. Acta*, 2013, **87**, 317–322.

26 X. Qi, H. Gao, Y. Zhang, X. Wang, Y. Chen and W. Sun, Electrochemical DNA biosensor with chitosan-Co_3O_4 nanorod-graphene composite for the sensitive detection of staphylococcus aureus nuc gene sequence, *Bioelectrochemistry*, 2012, **88**, 42–47.

27 Y. Niu, H. Xie, G. Luo, W. Weng, C. Ruan, G. Li and W. Sun, Electrochemical performance of myoglobin based on TiO_2-doped carbon nanofiber decorated electrode and its applications in biosensing, *RSC Adv.*, 2019, **9**, 4480–4487.

28 Y. Zhao, W. Ran, J. He, Y. Huang, Z. Liu, W. Liu, Y. Tang, L. Zhang, D. Gao and F. Gao, High-performance asymmetric supercapacitors based on multilayer MnO_2/graphene oxide nanoflakes and hierarchical porous carbon with enhanced cycling stability, *Small*, 2015, **11**, 1310–1319.

29 L. Li, Z. Du, S. Liu, Q. Hao, Y. Wang, Q. Li and T. Wang, A novel nonenzymatic hydrogen peroxide sensor based on MnO_2/graphene oxide nanocomposite, *Talanta*, 2010, **82**, 1637–1641.

30 Y. R. Chen, K. F. Chiu, H. C. Lin, C. L. Chen and C. Y. Hsieh, Graphene/activated carbon supercapacitors with sulfonated-polyetheretherketone as solid-state electrolyte and multifunctional binder, *Solid State Sci.*, 2014, **37**, 80–85.

31 C. J. Jafta, F. Nkosi, L. L. Roux, M. K. Mathe, M. Kebede, K. Makgopa, S. Yang, D. Tong, M. Oyama and N. Manyala, Manganese oxide/graphene oxide composites for high-energy aqueous asymmetric electrochemical capacitors, *Electrochim. Acta*, 2013, **110**, 228–233.

32 C. Yuan, H. Lin, H. Lu, E. Xing, Y. Zhang and B. Xie, Synthesis of hierarchically porous MnO_2/rice husks derived

carbon composite as high-performance electrode material for supercapacitors, *Appl. Energy*, 2016, **178**, 260–268.

33 H. Xie, X. Li, G. Luo, Y. Niu and G. Li, Nano-diamond modified electrode for the investigation on direct electrochemistry and electrocatalytic behavior of myoglobin, *Diamond Relat. Mater.*, 2019, **97**, 107453.

34 J. Liu, H. Cheng, H. Xie, G. Luo and W. Sun, Platinum nanoparticles decorating a biomass porous carbon nanocomposite-modified electrode for the electrocatalytic sensing of luteolin and application, *RSC Adv.*, 2019, **9**, 33607–33616.

35 H. Xie, G. Luo, Y. Niu, W. Weng and W. Sun, Synthesis and utilization of Co_3O_4 doped carbon nanofiber for fabrication of hemoglobin-based electrochemical sensor, *Mater. Sci. Eng., C*, 2020, **107**, 110209.

36 R. Zou, X. Li, G. Luo, Y. Niu, W. Weng, W. Sun, J. Xi, Y. Chen and G. Li, Boron nitride nanosheet modified electrode: preparation and application to direct electrochemistry of myoglobin, *Electroanalysis*, 2019, **31**, 575–581.

37 W. Sun, Y. Wang, Y. Zhang, X. Ju and Z. Sun, Poly(methylene blue) functionalized graphene modified carbon ionic liquid electrode for the electrochemical detection of dopamine, *Anal. Chim. Acta*, 2012, **751**, 59–65.

38 S. Xiong, X. Zhang, J. Chu, X. Wang, R. Zhang, M. Gong and B. Wu, Hydrothermal synthesis of porous sugarcane bagasse carbon/MnO_2 nanocomposite for supercapacitor application, *J. Electron. Mater.*, 2018, **47**, 6575–6582.

39 W. Chen, W. Weng, X. Niu, X. Li, Y. Men, W. Sun, G. Li and L. Dong, Boron-doped graphene quantum dots modified electrode for electrochemistry and electrocatalysis of hemoglobin, *J. Electroanal. Chem.*, 2018, **823**, 137–145.

40 K. B. Oldham, Analytical expressions for the reversible Randles-Sevcik function, *J. Electroanal. Chem.*, 1979, **105**, 373–375.

41 E. Laviron, General expression of the linear potential sweep voltammogram in the case of diffusionless electrochemical systems, *J. Electroanal. Chem.*, 1979, **101**, 19–28.

42 X. Chen, Z. Wang, F. Zhang, L. Zhu, Y. Li and Y. Xia, Determination of rutin on the poly(p-aminobenzene sulfonic acid) modified glassy carbon electrode, *Chem. Pharm. Bull.*, 2010, **58**, 475–478.

43 S. Wei, X. Wang, H. Zhu, X. Sun, S. Fan, G. Li and Z. Sun, Graphene-MnO_2 nanocomposite modified carbon ionic liquid electrode for the sensitive electrochemical detection of rutin, *Sens. Actuators, B*, 2013, **178**, 443–449.

44 Ş. U. Karabiberoğlu and Z. Dursun, Fabrication of nickel coated graphene oxide composite electrode for sensitive determination of Rutin, *J. Electroanal. Chem.*, 2018, 76–85.

45 S. Li, B. Yang, C. Wang, W. Jin, F. Yue, Y. Bo, Z. Xiong and Y. Du, A facile and green fabrication of Cu_2O-Au/NG nanocomposites for sensitive electrochemical determination of rutin, *J. Electroanal. Chem.*, 2017, **786**, 20–27.

46 B. B. Yang, D. Bin, K. Zhang, Y. Du and T. Majima, A seed-mediated method to design N-doped graphene supported gold-silver nanothorns sensor for rutin detection, *J. Colloid Interface Sci.*, 2018, **512**, 446–454.

47 R. Xing, H. Yang, S. Li, J. Yang, X. Zhao, Q. Wang, S. Liu and X. Liu, A sensitive and reliable rutin electrochemical sensor based on palladium phthalocyanine-MWCNTs-Nafion nanocomposite, *J. Solid State Electrochem.*, 2016, **21**, 1–10.

48 J. L. He, Y. Yang, X. Yang, Y. L. Liu, G. L. Shen and R. Q. Yu, β-Cyclodextrin incorporated carbon nanotube-modified electrode as an electrochemical sensor for rutin, *Sens. Actuators, B*, 2006, **114**, 94–100.

49 S. H. Nile, A. S. Nile, Y. S. Keum and K. Sharmab, Utilization of quercetin and quercetin glycosides from onion (Allium cepa L.) solid waste as an antioxidant, urease and xanthine oxidase inhibitors, *Food Chem.*, 2017, **235**, 119–126.

